The Astronomical Journal, 157:113 (15pp), 2019 March https://doi.org/10.3847/1538-3881/aaf477
© 2019. The American Astronomical Society. All rights reserved.

Predicted Number, Multiplicity, and Orbital Dynamics of *TESS* M-dwarf Exoplanets

Sarah Ballard[1]
MIT Kavli Institute for Astrophysics & Space Research, Cambridge, MA 02139, USA; sarahba@mit.edu
Received 2018 January 15; revised 2018 October 7; accepted 2018 November 1; published 2019 February 12

Abstract

We present a study of the M-dwarf exoplanetary systems forthcoming from NASA's *TESS* mission. While the mission's footprint is too complex to be characterized by a single detection completeness, we extract ensemble completeness functions that recover the planet detections from previous work for stars between 3200 and 4000 K. We employ these completeness functions, together with a dual-population planet occurrence model that includes compact multiple planetary systems, to infer anew the planet yield. We predict both the number of M-dwarf planets likely from *TESS* and their system architectures. We report four main findings. First, *TESS* will likely detect more planets orbiting M dwarfs that previously predicted. Around stars with effective temperatures between 3200 and 4000 K, we predict that *TESS* will find 1274 ± 241 planets orbiting 1026 ± 182 stars, a 1.2-fold increase over previous predictions. Second, *TESS* will find two or more transiting planets around 20% of these host stars, a number similar to the multiplicity yield of NASA's *Kepler* mission. Third, *TESS* light curves in which one or more planets are detected will often contain transits of additional planets below the detection threshold of *TESS*. Among a typical set of 200 *TESS* hosts to one or more detected planets, 93 ± 17 transiting planets will be missed. Transit follow-up efforts with the photometric sensitivity to detect an Earth or larger around a mid-M dwarf, even with very modest period completeness, will readily result in additional planet discoveries. Fourth, the strong preference of *TESS* for systems of compact multiples indicates that *TESS* planets will be dynamically cooler on average than *Kepler* planets, with 90% of *TESS* planets residing in orbits with $e < 0.15$. We include both (1) a predicted sample of planets detected by *TESS* orbiting stars between 3200 and 4000 K, including additional nontransiting planets, or transiting and undetected planets orbiting the same star and (2) sample completeness functions for use by the community.

Key words: eclipses – planetary systems – planets and satellites: detection

Supporting material: machine-readable table, tar.gz file

1. Introduction

NASA's *TESS* mission (Ricker et al. 2014) will furnish the vast majority of small, rocky planets for atmospheric study. A typical *TESS* target star receives 27 days of continuous observation, so the sensitivity of the mission strongly favors short periods (Sullivan et al. 2015). A handful of transits of a small planet will be detectable over this duration only if those transits are individually large, which is why 75% of small planets detected by *TESS* are expected to orbit M dwarfs (Sullivan et al. 2015). In fact, it is likely that every small planet discovered by *TESS* to reside in its star's habitable zone will orbit an M dwarf (Sullivan et al. 2015). Combining this fact with the favorable signal-to-noise ratio of a planetary transmission spectrum around a small star (Tarter et al. 2007), M dwarfs will likely be the majority of sites for focused follow-up atmospheric study in the next decade with the *James Webb Space Telescope* (*JWST*; Gardner et al. 2006). The forthcoming *TESS* sample of planets orbiting M dwarfs will likely contain many targets of the first biosignature searches. The discovery of planets with *TESS* has already begun, with only the second published planet orbiting the M dwarf LHS 3844 (Vanderspek et al. 2018).

The ensemble of planets orbiting M dwarfs has come into focus from a combination of radial velocity, microlensing, high-contrast imaging, and transit surveys (Johnson et al. 2010; Bonfils et al. 2013; Dressing & Charbonneau 2013, 2015; Montet et al. 2014; Morton & Swift 2014; Bowler et al. 2015; Muirhead et al. 2015; Clanton & Gaudi 2016; for a detailed summary, see Shields et al. 2016). In particular, the photometric sensitivity of NASA's *Kepler* mission illuminated the population of planets smaller than 4 $R_{\oplus}$ in orbit around M dwarfs, showing that they are more common around late spectral types than around FGK dwarfs (Howard et al. 2012; Mulders et al. 2015). They are so common, in fact, that Morton & Swift (2014) found 2.00 ± 0.45 planets per M dwarf, and Dressing & Charbonneau (2015) reported a similar value of 2.5 ± 0.2 planets per star.

Yet M-dwarf planetary systems resist a simple, one-population explanation. An occurrence rate of two to three planets per M dwarf (Morton & Swift 2014; Dressing & Charbonneau 2015) recovers the raw number of planets detected by *the Kepler* mission, but it furnishes only a fair fit to the properties of those detected planets, like the number of transiting planets per star (Ballard & Johnson 2016). The top panels of Figure 1 show the result of using one mode of planet occurrence, in comparison with the observed *Kepler* parameters. One explanation is that the model of two to three planets per star, with the underlying period and radius distribution in Dressing & Charbonneau (2015), is in fact an average of two very different types of planetary systems. Observations of orbital eccentricity and spin–orbit alignment indicate that the systems with one transiting planet are dynamically distinct from those with two or more transiting planets. Planets in multiple-planet systems reside in more circular orbits (Xie et al. 2016) and are more aligned with the spins of their host stars (Morton & Winn 2014). The number of

[1] MIT Torres Fellow for Exoplanetary Science.

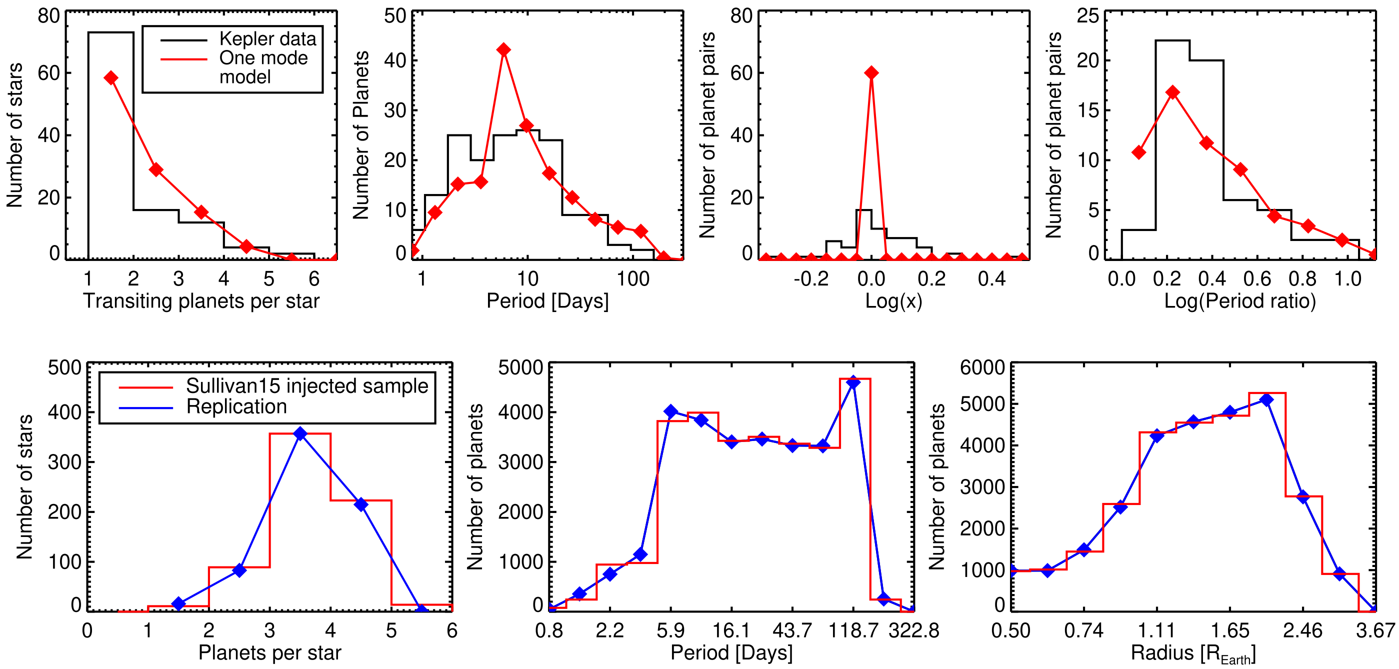

Figure 1. Top panels: observed *Kepler* distributions (black) of detected planets in the number of transiting planets per star, period, transit duration ratio (ξ defined in Fabrycky et al. 2012b), and period ratio. Overplotted in red is the best one-mode planet occurrence model, with 2.5 planets per star drawn from Dressing & Charbonneau (2015). The delta function in ξ in the third panel is due to uniformly applying an orbital mutual inclination of 0°. Bottom panels: consistency in the underlying distributions of the number of planets per star, periods, and radii of our one-mode model (blue) to the values used in Sullivan et al. (2015). The number of planets per star is drawn from Table 6 of that work, and the planetary radii and period distributions are drawn from Figure 8 of Sullivan et al. (2015).

transiting planets per star from *Kepler* also indicates two populations with different dynamical properties: one with at least five planets coplanar to within 2° and the other with one to two planets at larger orbital inclinations with respect to one another (Ballard & Johnson 2016). This two-population model removes the discrepancy in the top left panel of Figure 1, in which the number of systems with only one transiting planet is underestimated, and the number of systems with two transiting planets is overestimated in equal measure. The two-population model also furnishes a better fit to other observables, like period, period ratio, and transit duration ratio (Dawson et al. 2016; Moriarty & Ballard 2016). While the so-called "*Kepler* dichotomy" (Lissauer et al. 2011) explanation is not definitive, nor is it the only one (Gaidos et al. 2016; Bovaird & Lineweaver 2017), we employ it here as a useful phenomenological descriptor of M-dwarf planetary systems.

This two-mode model is also consistent with the independent measurement of the rate of "compact multiples." These are systems with at least two planets with orbital periods less than 10 days. Muirhead et al. (2015) showed that at least 20% of M dwarfs host a compact multiple system, and that fraction increases as stellar temperature decreases. Within the two-population framework, these compact multiples are recognizable as the systems with more than five planets per star interior to 200 days. As we described above, compact multiples need to be included in order to reproduce the *Kepler* yield (Ballard & Johnson 2016). Similarly, their inclusion should also result in a more realistic prediction of the *TESS* yield.

A sophisticated study of the likely *TESS* planet yield, employing the 2 minute cadence mode, across the FGKM spectral types by Sullivan et al. (2015) incorporated the complicated *TESS* footprint, its instrumental limitations, the range of noise budgets within the surveyed stellar population, and false-positive likelihoods. We do not aim to replicate the Sullivan et al. (2015) machinery in its complexity; because of that study, we already have an excellent understanding of how *TESS* will respond to incoming photons. Rather, we propose to extend the analysis, specifically for the M dwarfs. First, we will extract from Sullivan et al. (2015) the completeness function for M dwarfs from 3200 to 4000 K as a function of orbital period and planet radius. Then, we will apply that completeness function, with a difference occurrence model, to predict anew the *TESS* yield of planets orbiting M dwarfs. We undertake these steps for the following reasons.

First, Sullivan et al. (2015) employed a one-mode model of planet occurrence, one that does not include "compact multiple" systems with at least two planets with orbital periods <10 days. We hypothesize that a planet occurrence rate that includes these systems will change the predicted yield in important ways. Given the short, 27 day baseline of observations for most *TESS* stars, these types of systems will be much more likely to furnish a transit within those 27 days. "Compact multiples" are likelier to host multiple transiting planets too, both because the transit probabilities are higher for each individual planet in these close-in orbits and because these systems are coplanar within 1°–2° as a rule (Fabrycky et al. 2012b). For these reasons, we hypothesize that a predicted *TESS* yield that includes compact multiples will differ from the Sullivan et al. (2015) sample as follows.

1. The sample will contain more planet detections.
2. It will find that *TESS* will detect two or more transiting planets around a substantial number of stars.
3. It will find that the *TESS* light curves with a detected planet will very often contain transits of additional planets lurking below the noise.

Second, the *TESS* completeness function for planets orbiting M dwarfs as a function of radius and period is useful in its own right. This function is not included in the Sullivan et al. (2015) study but is readily extractable from it. Transit occurrence rate studies rely on completeness as a function of radius and period (e.g., Howard et al. 2012; Berta et al. 2013; Dressing & Charbonneau 2013; Petigura et al. 2013a). Providing the approximate *TESS* M-dwarf completeness to the community will enable occurrence rate science even with early *TESS* detections. In addition, a comparison between this predicted completeness function and the actual completeness function for the mission will be illuminating. It will encode the differences between predicted and actual sources of both instrumental and stellar noise.

We organize this study as follows. In Section 2, we describe our analysis, including the generation of synthetic planetary systems (Section 2.1) and how we create a mixture model of planetary systems (Section 2.2). Section 2.3 describes the extraction of the M-dwarf completeness function for *TESS*, and Section 2.4 describes how we apply it to the mixture model. Section 3 contains the results of this exercise. We enumerate the following goals for this study, which are addressed in the indicated sections.

1. Repredict the number of planet detections among M dwarfs observed by *TESS* (Section 3.1).
2. Determine how often *TESS* will detect a single transiting planet and how often it will detect two or more planets transiting the same M dwarf (Section 3.2).
3. Determine which additional planets, if any, will transit known *TESS* M-dwarf planet host stars but elude detection in *TESS* light curves (Section 3.3).
4. Predict the fraction of *TESS*-detected systems that will have "compact multiple" architecture, as compared to the underlying rate in nature (Section 3.4).
5. Predict the eccentricity distribution of the detected *TESS* planets and compare it to that of *Kepler* M-dwarf planets (Section 3.5).
6. Approximate the number of planets orbiting M dwarfs that *TESS* will detect that will exhibit transit-timing variations (TTVs) using the rate of TTV occurrence measured by *Kepler* (Section 3.6).
7. Make a prediction for the bulk densities of planets detected by *TESS* from planet formation theory and compare these densities to the densities inferred for the *Kepler* planets (Section 3.7.)

In Section 4, we summarize our findings and conclude.

2. Analysis

2.1. Generating Planetary Systems

To generate a realistic synthetic sample of planetary systems, we take the following steps. We draw periods and radii for each mock planetary system from the empirical distribution of Dressing & Charbonneau (2015). We then employ the distributions of Limbach & Turner (2015) to assign eccentricity. We assign planetary masses with the relations of Zeng & Jacobsen (2017) for $R < 1.5\,R_\oplus$ and Wolfgang et al. (2016) for $R > 1.5\,R_\oplus$. Rogers (2015) identified the cutoff between a majority of rocky planets and a majority of icy/gaseous planets at $1.5\,R_\oplus$, but these two relations also naturally overlap at $1.5\,R_\oplus$. We assess the stability of the system by ensuring that planets satisfy the criterion defined in Fabrycky et al. (2012b),

$$\Delta \equiv (a_2 - a_1)/R_{\mathrm{H}_{1,2}} > 2\sqrt{3}\,, \quad (1)$$

where the mutual Hill radius $R_{\mathrm{H}_{1,2}}$ is defined by

$$R_{\mathrm{H}_{1,2}} = \left[\frac{M_1 + M_2}{3M_\star}\right]^{1/3}\frac{(a_1 + a_2)}{2}. \quad (2)$$

This criterion is applicable for circular orbits. For eccentric orbits, we calculate the periapse and apoapse separation from the host star for each planet. We assume the orbits are stable if Equation (1) holds for the apoapse distance of the inner planet and the periapse of the outer planet. For generating synthetic *TESS* planetary systems orbiting M dwarfs, we employ four different stellar masses corresponding to four different effective temperature ranges (from Boyajian et al. 2012): 0.25 $M_\odot$ (for stars 3200–3400 K), 0.41 $M_\odot$ (for stars 3400–3600 K), 0.50 $M_\odot$ (for stars 3600–3800 K), and 0.60 $M_\odot$ (for stars 3800–4000 K).

We then assign a Boolean TTV flag to each transiting planet. Xie et al. (2014) showed that planets drawn from multi-transiting systems are likelier to exhibit TTVs, with that likeliness increasing as the number of transiting planets increases. We assign the TTV probability per planet from that work, as defined by their "Case 3" (the most generous TTV occurrence rate): 3.5% for planets in singly transiting systems, 7% for planets in doubly transiting systems, 8% for planets in triply transiting systems, and 10.4% for planets in systems with four or more transiting planets.

Finally, we calculate and record an independent density for each planet using only its mutual Hill spacing from neighboring planets. Dawson et al. (2016) predicted a theoretical relationship between these parameters: $\rho\ [\mathrm{g\ cm^{-3}}] = (\Delta/22)^6$, where Δ is defined in Equation (1). The scaling of density with mutual Hill separation provides a natural explanation, among others, for the fluffier nature of planets whose masses were measured with TTVs (Wolfgang et al. 2016; Mills & Mazeh 2017).

2.2. Generating Mixture Models

In the simplified "*Kepler* dichotomy" model, stars host one of two distinct types of planetary systems. Ballard & Johnson (2016) showed that the *Kepler* M-dwarf planets are well described by one population of stars hosting flat and manifold systems of planets (with the number of planets per star N at least five and orbital mutual inclinations σ between 1° and 3°), with the other hosting one or two planets with high mutual inclination (>8°). Throughout this work, we refer to the former type of planetary system as "Population 1" or, more descriptively, as a "compact multiple." That work investigated the mixture specifically among detected planet hosts: in reality, the former type of planetary system is overly represented among detected planet hosts. This is because the typical short periods within the multiple systems make it likelier that at least one planet will transit. The degree of this overrepresentation in both *Kepler* and *TESS* is discussed in Section 3.4.

We define N as the number of planets per star and σ as the width of the Rayleigh distribution from which we draw their mutual inclinations. For a set of $\{N, \sigma\}$, we generate 10^4 planetary systems using the criteria established in Section 2.1, employing the posterior distributions on these quantities from Ballard & Johnson (2016). We then determine, based upon the assumption of random alignments for each planetary system with the line of sight, which planets transit their host star. We consider noninteger N as follows. If a "typical" planetary system defined by N and σ hosts 3.5 planets, then 50% of stars host three planets (with eccentricities drawn from the cumulative distribution function (CDF) for three-planet systems) and 50% host four (with eccentricities drawn from the CDF for four-planet systems).

The fraction f of stars in Population 1 in Ballard & Johnson (2016) is the fraction of transiting systems in Population 1, not the fraction of stars. For each f, we now calculate an $f_{\star}$, the fraction of stars in Population 1 necessary to recover a contribution f to the total number of transiting systems. For mixture models defined by the set $\{N_1, \sigma_1, N_2, \sigma_2, f_{\star}\}$, we randomly select $10^4 \cdot f_{\star}$ stars populated by $\{N_1, \sigma_1\}$ and $10^4 \cdot (1\text{-}f_{\star})$ stars populated by $\{N_2, \sigma_2\}$. We then draw properties from the transiting planets among this final set of 10^4 stars. Of course, the vast majority of these stars host zero transiting planets.

2.3. Extracting the TESS Completeness Function

To determine what a transit mission will detect, it is useful to know how often any given transiting planet will be detected, typically as a function of radius and orbital period. This quantity is the "completeness," and it is, in principle, distinct for every star the mission surveys. In the absence of real light curves, Sullivan et al. (2015) used a signal-to-noise criterion to evaluate whether injected planets would be "detected" by *TESS*. The stare-and-step observation strategy of *TESS* means that most stars in the mission footprint receive 27 days of continuous photometry. However, overlap between observing fields results in some stars residing for up to a year in the field of view. Sullivan et al.'s (2015) study incorporated the full complexity of the *TESS* footprint and its stellar sample. The completeness of the survey to planets of a given size and period is not included in the study but is derivable from it as follows.

Given the Sullivan et al. (2015) sample of injected planets (which we can recreate from descriptions in that work) and the sample of detected planets reported in their Table 6 (here known as the "data"), we can recover the completeness function that maps one to the other. We elect to fit this completeness function at four points across the M spectral type: for stars between 3200 and 3400, 3400 and 3600, 3600 and 3800, and 3800 and 4000 K. We hypothesize that the completeness for 4000 K ought to not differ greatly from the completeness at 3200 K from *TESS*. There is the advantage of a deeper transit depth for smaller stars; a factor of 4 difference between a 0.25 $R_{\odot}$ star and 0.5 $R_{\odot}$ star (bracketing the approximate range of these temperatures per Boyajian et al. 2012) for the same size planet. However, this increased transit depth for a 0.25 $M_{\odot}$ star is offset by a shorter transit duration ($\sim$0.6$\times$ as long) and by the fact that it is, on average, dimmer by 2 mag in the *TESS* sample. We anticipate that completeness should be higher by about 20% for a given planet size for the lowest-temperature bin as compared to the highest.

2.3.1. Replication of Sullivan Sample

We first create a sample of injected planets using the criteria described in Sullivan et al. (2015). We employ the same population of M dwarfs from 3200 to 4000 K shown in their Figure 17, with stellar radius and mass assigned for each temperature range from Boyajian et al. (2012), Equations (8) and (10), respectively. This sample includes 27,000 stars between 3200 and 3400 K (we employ a mass of 0.25 $M_{\odot}$ and a radius of 0.25 $R_{\odot}$ for these stars), 25,000 stars between 3400 and 3600 K ($M = 0.41$ $M_{\odot}$, $R = 0.39$ $R_{\odot}$), 10,000 stars between 3600 and 3800 K ($M = 0.50 M_{\odot}$, $R = 0.49\, R_{\odot}$), and 6000 stars between 3800 and 4000 K ($M = 0.6 M_{\odot}$, $R = 0.56$ $R_{\odot}$). For each of the four effective temperature ranges, we assign planets to each star per Sullivan et al. (2015), with a process similar to the one described in Section 2.1 for a single mode of planet occurrence. However, the Sullivan et al. (2015) process that we replicate here differs in that (1) they assign more than one planet to a given star with independent probability, rather than assigning the number of planets per star a priori, and (2) they assume a mutual inclination between orbits of zero. The sample of injected planets from Sullivan et al. (2015) was generated at fixed resolution in both log (period) and log(radius) (inherited from Youdin 2011; Howard et al. 2012; Dressing & Charbonneau 2013, and others), with an approximate spacing of 1 dex between adjacent log(period) bins and 0.2 dex between adjacent log(radius) bins. Because we cannot expect to extract information at a higher resolution than these values, we adopt their spacing. In practice, the index i spans periods from 0.8 to 320 days in 13 regular log intervals of 1 dex, and the index j spans radii from 0.3 to 4 $R_{\oplus}$ in 17 regular log intervals of 0.2 dex.

In the bottom panels of Figure 1, we show consistency between the sample we generated from the stated criteria and the one employed in Sullivan et al. (2015; see their Figure 8).

2.3.2. Definition of Terms

From this sample of stars and planets generated in the same way as Sullivan et al. (2015), we assume random orientation of the mean orbital plane on the sky. We identify which of the planets in this sample transit and call this injected sample of planets $N_{i,j}$, where i is the index of the period bin and j is the index of the radius bin. We treat each individual bin at this resolution as a bucket that holds an integer number of planets.

We aim now to find the completeness function that winnows this injected sample of transiting planets $N_{i,j}$ to the detected sample reported by Sullivan et al. (2015) in Table 6. Using the same log spacing, we designate $D_{i,j}$ the number of detected planets per bin. The actual surfaces of both $D_{i,j}$ and $N_{i,j}$ are shown in the top two panels of Figure 2 and individually as a function of radius and period in Figure 3 (with injected transiting planets N in black and detected planets D in red). These two quantities are related by the completeness $C_{i,j}(\Theta)$, some as yet unknown function that encodes the probability that a given injected transiting planet–planet will be detected by *TESS*. This completeness is defined by a set of parameters Θ. In past studies, completeness is often evaluated in each bin empirically from injection-and-recovery studies. This is performed either in an average sense (e.g., Petigura et al. 2013b) or separately for each individual star in the sample (Dressing & Charbonneau 2015; Christiansen et al. 2016). Here we propose to use Bayesian forward modeling, assuming a functional form for C. The advantages of Bayesian forward modeling for completeness and occurrence rate studies are enumerated in detail in Foreman-Mackey et al. (2014) and Hsu et al. (2018). If we select a given completeness function and wish to know its likelihood, we can produce a model "detected" data set and compare it to the data set presented

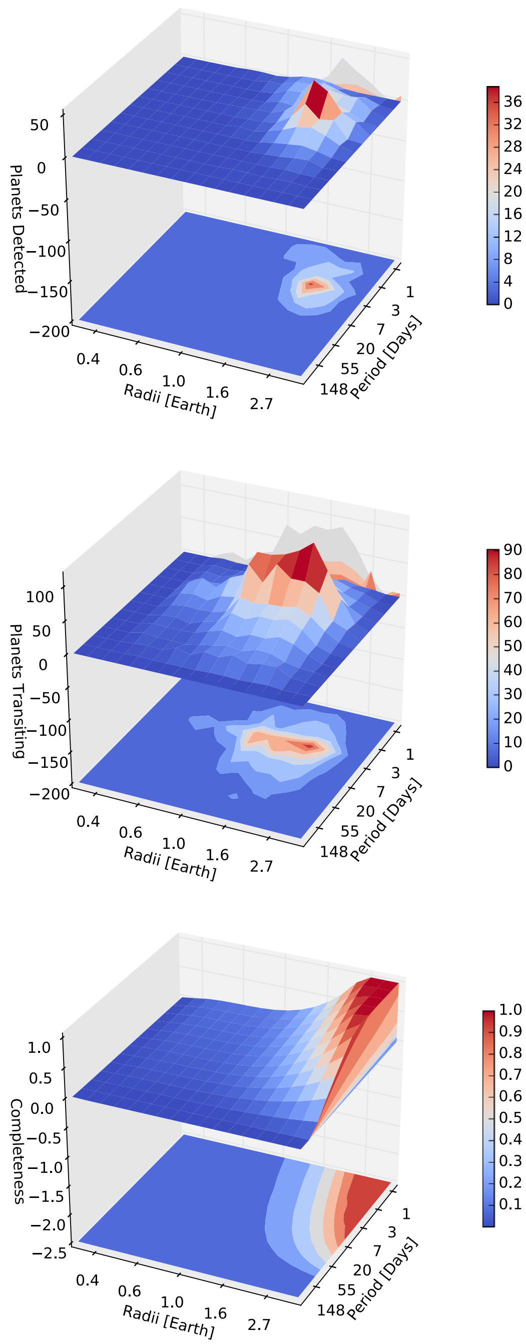

Figure 2. Top panel: detected planets $D_{i,j}$ from Sullivan et al. (2015). Middle panel: injected transiting planets sample generated using the criteria from the same, $N_{i,j}$. Bottom panel: typical polynomial completeness function evaluated at each bin, $C_{i,j}$.

in Sullivan et al. (2015). This model will be the number of planets injected in each bin $N_{i,j}$, weighted by the probability of detection $C_{i,j}(\Theta)$, and we designate it $\mu_{i,j}(\Theta)$, our guess at the number of planets in each bin that ought to be detected:

$$\mu_{i,j}(\Theta) = N_{i,j} \cdot C_{i,j}(\Theta). \tag{3}$$

Within a Bayesian framework,

$$P(\Theta|D) \propto \mathscr{L}(\Theta)\pi(\Theta), \tag{4}$$

where $P(\Theta|D)$ is what we wish to know: the probability of a set of model parameters Θ, given the observed data D. The likelihood $\mathscr{L}(\Theta)$ is the probability of the data D being observed, given a set of model parameters Θ, while $\pi(\Theta)$ represents our prior knowledge of Θ.

Poisson counting statistics describe integer numbers of transiting planets, so we evaluate the likelihood of Θ with a Poisson likelihood function. This likelihood is conditioned on the "observed" number of planets detected in that bin, $D_{i,j}$,

$$\mathscr{L} \propto \prod_i \prod_j \frac{\mu_{i,j}(a)^{D_{i,j}} e^{-\mu_{i,j}(a)}}{D_{i,j}!}, \tag{5}$$

where $\mu_{i,j} = \mu_{i,j}(\Theta)$, our model for the number of detected planets in that bin, which depends upon the model parameter Θ, defined in Equation (3).

2.3.3. Functional Form for Completeness

We experimented with various functional forms for the completeness C. We adopt a smooth, analytic function for C, which we evaluate at the same resolution in log(period) and log (radius) to produce the completeness of each bin $C_{i,j}$. Trial versions of C included a single-to-noise scaling, as well as simple power laws in log period or radius. Neither of the two functions for completeness, when applied to the injected planets, correctly approximated the number of detected planets: for example, while the predicted number of short-period planets might match, long-period planets would be strongly underestimated. We elected to use a polynomial in log(radius) and log(period) for C, with some constraints.

First, we require the completeness to be separable in period and radius (that is, $C(P, R_p) = C(P) \cdot C(R_p)$, similar to Youdin 2011). We require that it be bounded between 0 and 1, and we require it to be monotonic (increasing with radius and decreasing with period). We ultimately adopted a third-degree polynomial in both log(radius) and log(period). For example, the completeness with radius $C(R_p)$ is defined by

$$C(R_p) = \Theta_1 + \Theta_2 R_p + \Theta_3 R_p^2 + \Theta_4 R_p^3. \tag{6}$$

This results in a total of eight free parameters for Θ: four coefficients for the completeness with orbital period $C(P)$ and four for the completeness with planet radius $C(R_p)$. There exists a linear algebra solution for finding $[\Theta_1, \Theta_2, \Theta_3, \Theta_4]$ for each polynomial, a modified version of the singular value decomposition adapted for monotonic polynomials that relies upon Lagrange multipliers (Hawkins 1994; Murray et al. 2013). The `MonoPoly` package in R (Turlach & Murray 2016) implements those tools, which we used as a first estimate for the coefficients Θ: four for $C(P)$ and four for $C(R_p)$. The third panel of Figure 2 shows this first estimate of the completeness.

2.3.4. Evaluating Likelihood

We employ the Bayesian sampler MultiNest (Feroz & Hobson 2008; Feroz et al. 2009, 2013, with Python implementation by Buchner et al. 2014) to evaluate these likelihoods and posterior distributions. In practice, MultiNest calculates the log of the likelihood defined in Equation (5). We use uniform priors for each of the polynomial coefficients, allowing them to vary to within 200% of the least-squares value. We enforce a monotonically decreasing polynomial in log period and a monotonically increasing polynomial in log radius by setting the log likelihood to an arbitrarily low value otherwise (-10^{-30} in our case, in comparison to a typical log likelihood of -300).

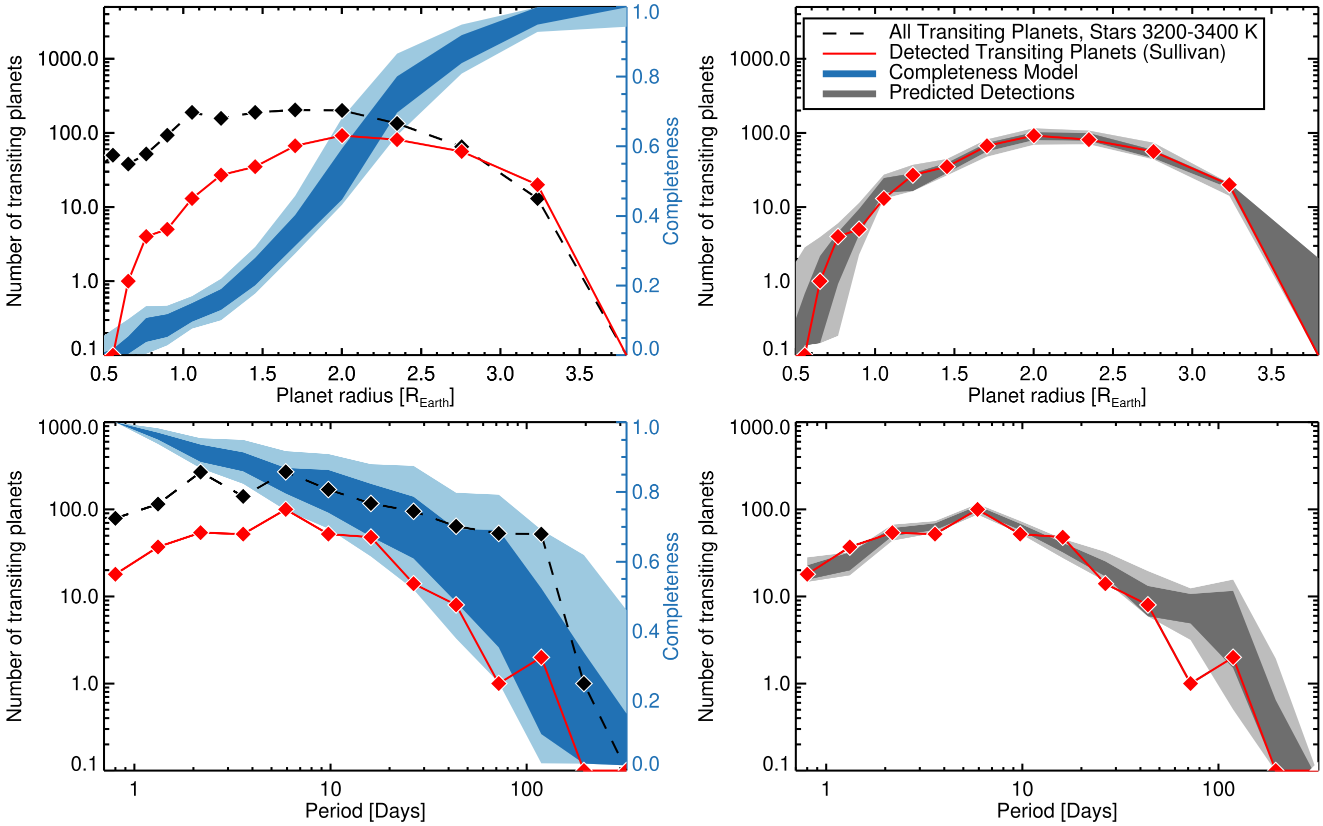

Figure 3. Left panels: injected transiting planets N (black) and detected planets D (red) from Sullivan et al. (2015) as a function of radius and period. Model completeness functions in radius and period are overplotted in dark (1σ) and light (2σ) blue; the right axis corresponds to completeness. Right panels: population of detected Sullivan et al. (2015) planets, now with models μ for predicted planet detections overplotted in gray.

Figure 3 summarizes the results of the completeness fit for one bin, 3400–3600 K. The injected transiting planets $N_{i,j}$ are shown in black as a function of radius (top panel) and period (bottom panel). The detected planets $D_{i,j}$ (Table 6 from Sullivan et al. 2015) are shown in red. Blue shows the completeness functions that best recover $D_{i,j}$ from $N_{i,j}$, which we draw from the posterior distribution in the coefficients Θ. The right-hand panels show the 1σ and 2σ confidence intervals on the model number of detected planets $\mu_{i,j}$ in gray. We verify that the extracted completeness is successful at recovering the number of detected planets from the injected planets of Sullivan et al. (2015). We note the large uncertainty of the completeness function at long periods: at 100 days, for example, completenesses of both 40% and 0% are consistent at 2σ confidence. This is due to the inherent Poisson noisiness of only a few (<10 planets) detections with which to constrain the completeness.

We compare the completeness functions across the range of stellar temperatures. For the 3200–3400 K ($0.25\,M_{\odot}$) and 3800–4000 K ($0.6\,M_{\odot}$) stars, Figure 4 shows the range of completeness with radius drawn from the 1σ confidence intervals in Θ. As predicted, there is about a 20% average enhancement in completeness for the smallest stars as compared to the largest. There is an exception for planets with radii $<1.0\,R_{\oplus}$: while the completeness is consistent with zero for stars 3800–4000 K, it is 0.10 ± 0.05 for stars 3200–3400 K.

We include a representative sample of completenesses drawn from the posterior distributions for Θ with this manuscript from each of the four stellar effective temperature ranges.

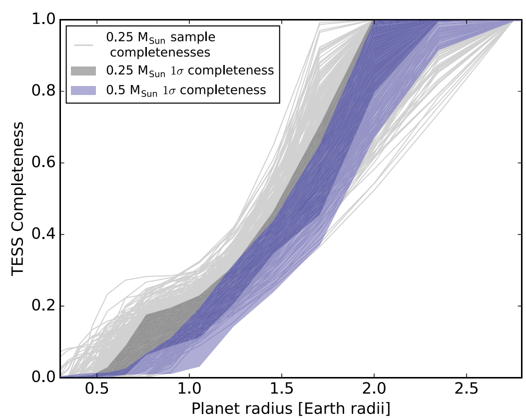

Figure 4. Comparison of completeness as a function of planet radius for spectral types M2V (gray) and M0V (purple). Individual draws from the M2V completeness posterior are shown in light gray, while the shaded regions depict areas of 1σ confidence.

2.4. Applying Completeness to Occurrence Mixture Model

With a *TESS* completeness function in hand, we can apply it to a new sample of simulated transiting planets, this time employing the mixture model in Ballard & Johnson (2016). As described in Section 2.1, we use the posteriors in the number of planets in both systems N_1 and N_2, their average mutual inclinations σ_1 and σ_2, and the fraction of host stars in the first population f directly from that work. The coefficients are highly correlated, so we cannot draw independently from their posterior distributions anew to sample the completeness. Rather, we save the completeness surface at each iteration of the Markov chain Monte Carlo (MCMC) chain. We have included these MCMC chains with this manuscript for use by the community.

For each transiting planetary system, we draw randomly from the sample of completeness surfaces $C_{i,j}$. For each individual planet's period and radius, we evaluate the detection likelihood from the completeness value corresponding to that bin. We take one additional step to enforce consistency for planets orbiting the same star, if both planets have orbital periods less than the 27 day observational baseline. A joint random draw of detection probabilities for multiple planets can occasionally result in the nonsensical scenario of less-likely planets being detected while more "detectable" planets are missed. We take as an example a system of two transiting planets: Planet 1 with a period and radius assigning it a 50% detection probability and Planet 2 with a radius and period assigning it a 5% detection probability. Out of 200 draws for a set of two random numbers between 0 and 1, there will be five instances in which Planet 2 is detected and Planet 1 is missed. This is a sensible scenario for an ensemble of stars, but for planets orbiting the same star, we consider the signal-to-noise ratios of the two planets (assume the same noise budget for both), and if the missed planet has a higher signal-to-noise ratio than the detected planet, we switch the former to "detected." This criterion moved 70 planets, on average, from "missed" to detected, out of a total of 3000 transiting planets in the sample as a whole.

We record the properties of each "detected" transiting planet, as well as its provenance (whether from a dynamically hot or cool configuration). For the sake of comparison, we repeat the exercise with the completeness function of *Kepler* (Dressing & Charbonneau 2015), so that we we can directly compare *Kepler* observables to those predicted for *TESS*. To generate synthetic *Kepler* systems, we employ a stellar mass $M_\star = 0.50\, M_\odot$.

3. Results

We revisit the goals enumerated in Section 1.

3.1. Summary of Planet Detections

In Figures 5 and 7, we show the resulting distribution of properties for the M dwarfs observed by the *Kepler* (gray) and *TESS* missions (blue, with the actual *Kepler* observables shown in red). The transit duration ratio, here denoted as ξ, is the one defined by Fabrycky et al. (2012a). For each parameter, we show the mean contribution to the total distribution from the dynamically cooler Population 1 (green) and dynamically hotter Population 2 (orange). The first immediately noticeable difference is in the period and radius distributions, where the effects of the *TESS* completeness are clear. *TESS* will skew heavily toward detecting larger planets than *Kepler* and at shorter orbital periods. We note that the mutual Hill spacing distribution shown in the second panel of Figure 7 is the true mutual spacing, not the (wider) spacing that would be measured only between detected planets.

In addition to the shapes of these distributions, it is useful to note the raw number of expected host stars and host planets. From the posterior distributions in the modeled number of detections $\mu_{i,j}$, we estimate that the *TESS* mission will find 1274 ± 241 planets orbiting 1026 ± 182 early-to-mid M-dwarf host stars. Unsurprisingly, given their strong representation among detected systems, the largest contribution to the uncertainty budget on the number of planets is the uncertainty on the fraction of planetary systems in compact multiples (see Section 3.4). We report in Table 1 how these total planet detections are distributed among the four stellar effective temperature ranges (defined in Section 2.3.1). In Figure 6, we show how the stars in each effective temperature range contribute to the total number of detections as a function of radius and period. We have superposed the 1σ confidence interval on the total number of detections with a dashed line to give a sense of the uncertainty on the number of detections as a function of period and radius. Table 2 contains a typical sample of "detected" planets, including the additional nontransiting or transiting but undetected planets orbiting the same star.

We note that the errors on the number of detected planets for individual stellar effective temperature bins do not sum in quadrature to the error on the total number of planets. This is because the numbers of detected planets in each effective temperature bin are highly correlated. If we employ a higher "compact multiple" fraction, it applies across all temperatures and corresponds to higher yields for all stars. Said a different way, the covariance between the numbers of detected planets in the different stellar temperature bins is nonzero: off-diagonal entries in the covariance matrix contribute half the total covariance.

We also investigate the subset of small, cool planets likely to be prioritized for follow-up with *JWST*. We define "small" here to be radii $<2R_\oplus$ and "cool" to be periods 20 days $< P <$ 40 days (approximating the habitable zone of an M3V dwarf). Among the 1274 ± 241 planets detected by *TESS*, 27 ± 3 meet these criteria. Critically for transit follow-up, an additional 28 ± 15 planets in this radius and period range are undetected but orbit stars for which *TESS* detected another planet. For the likeliest rocky planets with radii $<1.25R_\oplus$ in the same period range, *TESS* will detect 4^{+3}_{-2} (consistent with the three planets with radii $<1.5R_\oplus$ and orbital periods >20 days in the sample published in Sullivan et al. 2015). In even starker contrast with slightly larger planets, 21 ± 7 such planets will orbit known *TESS* hosts but elude detection by *TESS* proper. In the hypothetical situation where each known *TESS* M-dwarf host received 40 days of uninterrupted follow-up observation, the yield in newly uncovered temperate Earths would be triple or more that of *TESS* itself. It stands to reason that follow-up efforts with even moderate sensitivity at longer periods will uncover one or two of these, comparable to the number found in the mission data alone. We describe the follow-up implications in greater detail in Section 3.3.

3.2. Multiple Transiting Systems

Among these estimated 1,026,182 M-dwarf planet hosts identified by *TESS*, the mission will detect at least two planets around 189 ± 66 stars. The approximately 20% contribution of multis to the host star budget is similar to that of *Kepler* (see top panel of Figure 5). Even with the steepness of its completeness function with period, we predict that the mission will detect 45 ± 22 systems with three more or transiting planets, a number that makes intuitive sense given the fact that 20% of mid-M dwarfs host two or more planets interior to 10 days, and the average *TESS* star will receive 27 days of coverage.

Figure 8 shows a representative sample of *TESS* singles and multis, with a random selection of 20 systems from each population. Black circles, scaled to planet size, depict detections, while red circles are missed planets. The steep

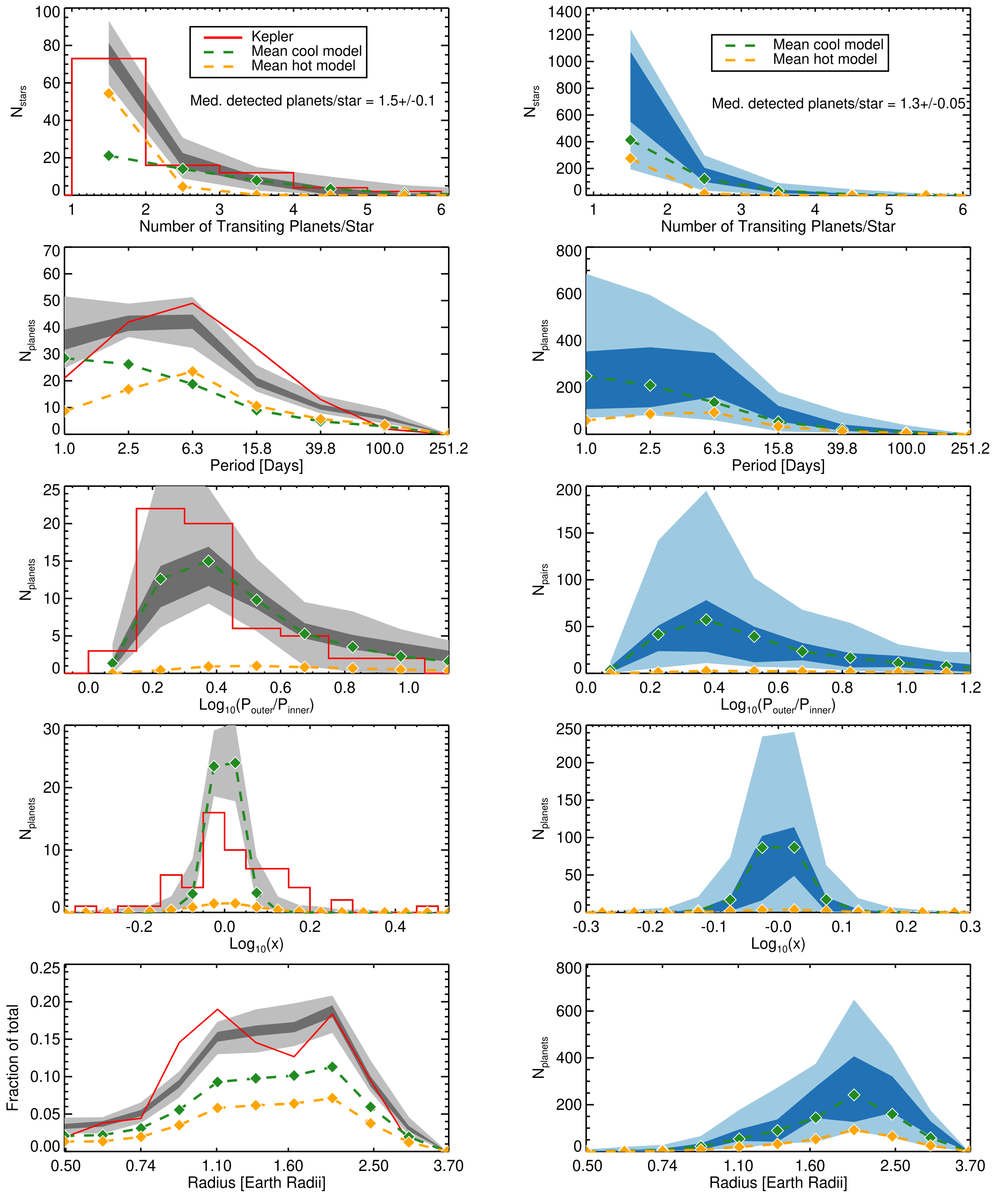

Figure 5. Resulting posterior distributions predicted for the *Kepler* mission at left (gray) and *TESS* mission at right. In order from top to bottom: number of detected transiting planets per star, periods of detected planets, period ratio between adjacent observed transiting planets, velocity-normalized transit duration ratio between adjacent planets, and planetary radius. All distributions have been normalized to compare to the shape of the actual observed *Kepler* distributions in red.

TESS radius completeness is especially visually evident here. We have indicated with blue circles the planets that exhibit TTVs, assigned from the Xie et al. (2014) occurrence rates as described in Section 2.1. The much higher rate of TTVs among multitransiting systems (even if only one planet was detected) is visually apparent: indeed, with a 3% occurrence of TTVs among singly transiting systems, none ought to appear in such a small representative sample. We note for clarity that we have shown 20 representative singly transiting and 20 representative multiply transiting systems as seen by *TESS* for a sense of their

Table 1
Summary of Planet Detections

T_{eff} (K)	$M_\star$ ($M_\odot$)	$R_\star$ ($R_\odot$)	Spectral Type[a]	N_{stars}	N_{hosts} (Stars)	$N_{detected}$ (Planets)	N_{missed} (Planets)	Detections Reported in S15
3200–3400	0.25	0.25	M3V, M4V	27,300	318 ± 98	383 ± 156	130 ± 77	328
3400–3600	0.41	0.39	M2V	25,000	393 ± 98	490 ± 134	191 ± 75	405
3600–3800	0.50	0.49	M1V	10,300	183 ± 43	231 ± 78	95 ± 32	158
3800–4000	0.60	0.56	M0V	6300	134 ± 40	170 ± 49	70 ± 33	113
All				68,900	1026 ± 182	1274 ± 241	484 ± 172	1024

Notes. Estimated *TESS* yields from this work for stars 3200–4000 K. Folding compact multiples into the planet occurrence rate increases the expected yield by 20% as compared to Sullivan et al. (2015; rightmost column). Here N_{missed} refers to the number of additional transiting planets orbiting the star either below the detection threshold or not transiting during the observational baseline.
[a] Approximate spectral types assigned from temperature from Boyajian et al. (2012), Table 12.

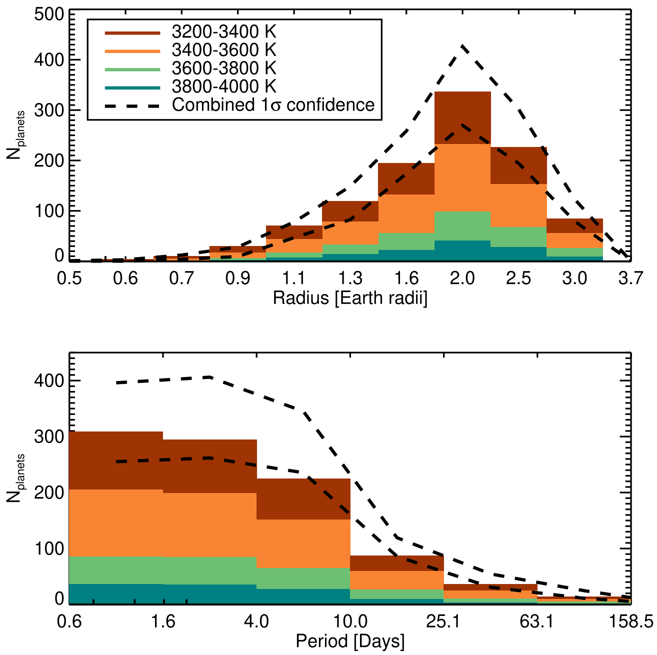

Figure 6. Detected planets for each spectral type as a function of planet radius (top panel) and orbital period (bottom panel). The 1σ confidence interval for the number of detections for the combined sample is shown with dashed lines.

architectures. However, 50:50 is not representative of their relative contributions to the total *TESS* yield as we describe above.

3.3. Implications for Transit Follow-up

The best-fit ensemble completeness function for *TESS* in the top left panel of Figure 3 has a critical implication specific to transit follow-up. As a whole, *TESS* will detect the transit of a 1.5 $R_\oplus$ planet orbiting an M dwarf 20% of the time (though the exact completeness depends on the period of the planet, as well as the spectral type). Comparing this modest likelihood with the occurrence rates of both Morton & Swift (2014) and Dressing & Charbonneau (2015; both of which show planets peaking in occurrence at 1–1.5 $R_\oplus$), it is clear that the majority of planets orbiting M dwarfs will lurk below the detection threshold. Yet the majority of stars around which *TESS* finds a planet will host a compact multiple system (primarily because of the steep period completeness function). For systems of three or more transiting planets, 40% of the time, *TESS* will detect only one planet, typically the very largest. This means that missed planets orbiting known *TESS* hosts will be remarkably common. We quantify this result in Figure 9, showing the number of missed planets per 200 *TESS* host stars (that is, stars for which *TESS* detected one or more planets). Among 200 *TESS* host stars, typically 250 planets will be detectable in the mission light curves themselves. But, on average, half that number lurk below the mission sensitivity: 93^{+17}_{-17} planets per 200 host stars. This is also visibly apparent in Figure 8, where missed (red) planets are common among their detected (black) neighbors.

Therefore, follow-up efforts sensitive to planets $<1.5\,R_\oplus$, even those with very modest period completeness, will readily find additional planets. For example, a hypothetical survey of 200 *TESS* hosts sensitive to 1 $R_\oplus$ planets with 100% completeness out to only 2.2 days will find an average of 11 additional planets (at least six, and as many as 16, within the 68% confidence interval). Especially promising for transit follow-up efforts: there are enough missed planets that surveys with 25% completeness at 40 days can expect to find at least one rocky (1–1.5 $R_\oplus$) planet in the habitable zone (for an M4V dwarf).

We point out the subtle but important distinction between the number of planets missed per 200 host stars and the number of those stars that host at least one missed planet. Among 200 hosts to at least one transiting planet, on average, 120 host only that transiting planet. Among the remaining 80 hosts, 50 host one missed planet, 20 host two, and 10 host three or more. The odds are statistically distinct for hosts to one *TESS*-detected planet versus multiple detected planets, as well as hosts to planets with detected TTVs. For the sake of illustration, among a sample of 200 systems where *TESS* detected at least two transiting planets, now, on average, 95 host at least one additional transiting planet. And, among a sample of 200 systems with a *TESS*-detected planet that also exhibits TTVs, the odds are yet more favorable: 112 hosts out of 200 will have additional unseen planets among them.

3.4. Underlying Occurrence Rate

We have employed the posterior distribution in *f* from Ballard & Johnson (2016), where *f* in that work is the fraction of transiting systems in the compact multiple configuration. However, because selection bias favors the detection of these systems, they are overrepresented among the *Kepler* host star sample compared to their true underlying fraction among stars. We aim to test for consistency with occurrence rate for compact multiples orbiting M dwarfs derived by Muirhead et al. (2015), though we approach the problem in different ways. First, the

Table 2
Mock Sample of Full Systems in Which *TESS* Detected at Least One Transiting Planet

Star ID	Planet ID	$T_{\rm eff}$ (K)	Vmag	Kmag	Distance (pc)	R.A.	Decl.	Period (days)	$a/R_\star$	i (deg)	Mass ($M_\oplus$)	Radius ($R_\oplus$)	Ω (deg)	Eccentricity	Hill Δ	Transit	Detected
1	1	3620	14.2	10.2	66.07	1.31	−24.9	2.01	11.7	2.46	12.1	3.2	48.3	0.103	11.13	1	1
1	2	3620	14.2	10.2	66.07	1.31	−24.9	3.56	17.1	1.76	3.3	1.4	161.6	0.014	13.53	1	1
1	3	3620	14.2	10.2	66.07	1.31	−24.9	6.37	25.2	1.47	2.2	1.3	11.1	0.047	21.88	1	0
1	4	3620	14.2	10.2	66.07	1.31	−24.9	16.51	47.6	2.53	2.1	1.2	297.9	0.044	22.14	0	−100
1	5	3620	14.2	10.2	66.07	1.31	−24.9	32.86	75.3	1.09	6.1	1.9	256.6	0.101	13.83	0	−100
1	6	3620	14.2	10.2	66.07	1.31	−24.9	56.94	108.6	1.99	7.4	2.2	59.1	0.025	15.38	0	−100
1	7	3620	14.2	10.2	66.07	1.31	−24.9	132.51	190.7	1.54	1.4	1.1	225.8	0.073	15.24	0	−100
1	8	3620	14.2	10.2	66.07	1.31	−24.9	184.97	238.2	0.11	2.0	1.2	294.5	0.033	10.92	1	0
2	1	3440	15.3	11.0	70.79	1.78	−71.9	2.44	14.9	0.91	9.8	2.7	137.1	0.067	51.32	1	1
2	2	3440	15.3	11.0	70.79	1.78	−71.9	87.01	161.7	0.24	0.4	0.8	215.4	0.454	51.32	0	−100
3	1	3230	15.1	10.4	23.44	1.79	−9.14	0.92	14.7	−3.06	9.3	2.6	200.8	0.071	18.01	1	1
3	2	3230	15.1	10.4	23.44	1.79	−9.14	2.42	28.0	−4.64	1.0	1.0	353.7	0.030	33.83	0	−100
3	3	3230	15.1	10.4	23.44	1.79	−9.14	8.68	65.5	−4.96	0.09	0.5	49.2	0.025	34.32	0	−100
3	4	3230	15.1	10.4	23.44	1.79	−9.14	16.43	100.2	−5.17	2.6	1.3	322.8	0.040	19.39	0	−100
3	5	3230	15.1	10.4	23.44	1.79	−9.14	37.43	173.4	−7.21	2.4	1.3	248.4	0.029	23.85	0	−100
3	6	3230	15.1	10.4	23.44	1.79	−9.14	109.09	353.9	−2.70	1.3	1.1	252.4	0.083	19.36	0	−100
3	7	3230	15.1	10.4	23.44	1.79	−9.14	188.22	509.0	−4.77	7.9	2.3	248.0	0.058	10.80	0	−100
4	1	3230	15.1	10.4	23.44	2.79	−8.14	2.53	28.8	0.14	5.9	1.8	341.8	0.141	16.39	1	1
4	2	3230	15.1	10.4	23.44	2.79	−8.14	6.88	56.1	−8.45	9.1	2.5	168.0	0.014	19.02	0	−100
4	3	3230	15.1	10.4	23.44	2.79	−8.14	34.32	163.7	−17.7	14.0	3.5	181.9	0.050	18.60	0	−100
4	4	3230	15.1	10.4	23.44	2.79	−8.14	95.38	323.6	−2.96	4.8	1.5	135.6	0.182	15.54	0	−100
5	1	3300	15.0	10.4	33.88	4.07	9.51	2.07	19.4	−5.61	4.0	1.5	336.0	0.090	20.53	0	−100
5	2	3300	15.0	10.4	33.88	4.07	9.51	6.36	41.1	12.43	6.6	2.0	118.7	0.209	19.65	0	−100
5	3	3300	15.0	10.4	33.88	4.07	9.51	21.05	91.3	0.24	9.9	2.7	344.4	0.206	20.70	1	1
5	4	3300	15.0	10.4	33.88	4.07	9.51	90.84	242.0	4.03	6.1	1.9	38.7	0.040	22.62	0	−100
6	1	3280	15.9	11.4	50.12	4.79	78.63	2.25	20.6	0.22	3.2	1.4	301.5	0.033	11.14	1	1
6	2	3280	15.9	11.4	50.12	4.79	78.63	4.00	30.2	2.05	6.6	2.0	72.4	0.076	14.86	0	−100
6	3	3280	15.9	11.4	50.12	4.79	78.63	9.92	55.3	2.77	1.3	1.1	260.5	0.011	14.21	0	−100
6	4	3280	15.9	11.4	50.12	4.79	78.63	15.33	73.9	0.17	5.0	1.6	139.0	0.053	12.19	1	0
6	5	3280	15.9	11.4	50.12	4.79	78.63	34.65	127.3	2.32	7.1	2.1	94.7	0.029	11.85	0	−100
6	6	3280	15.9	11.4	50.12	4.79	78.63	60.20	184.0	2.14	8.7	2.5	334.2	0.023	9.277	0	−100
6	7	3280	15.9	11.4	50.12	4.79	78.63	103.61	264.2	1.66	5.1	1.6	46.5	0.069	11.40	0	−100
6	8	3280	15.9	11.4	50.12	4.79	78.63	190.07	395.9	1.15	1.5	1.1	318.2	0.031	13.40	0	−100
7	1	3300	15.0	10.4	33.88	5.07	10.51	3.03	25.1	9.33	3.6	1.4	214.3	0.072	13.92	0	−100
7	2	3300	15.0	10.4	33.88	5.07	10.51	6.12	40.1	6.17	5.4	1.7	344.5	0.135	14.29	0	−100
7	3	3300	15.0	10.4	33.88	5.07	10.51	13.96	69.5	−0.69	6.8	2.0	350.9	0.061	12.35	1	1
7	4	3300	15.0	10.4	33.88	5.07	10.51	22.76	96.2	9.63	1.6	1.1	80.8	0.016	10.03	0	−100

Note. Typical yield of detected planets orbiting stars between 3200 and 4000 K observed by *TESS* in 2 minute cadence. We have also included additional planets orbiting the same star, both transiting (undetected) and nontransiting. The Hill spacing quantity Δ is defined in Equation (1).

(This table is available in its entirety in machine-readable form.)

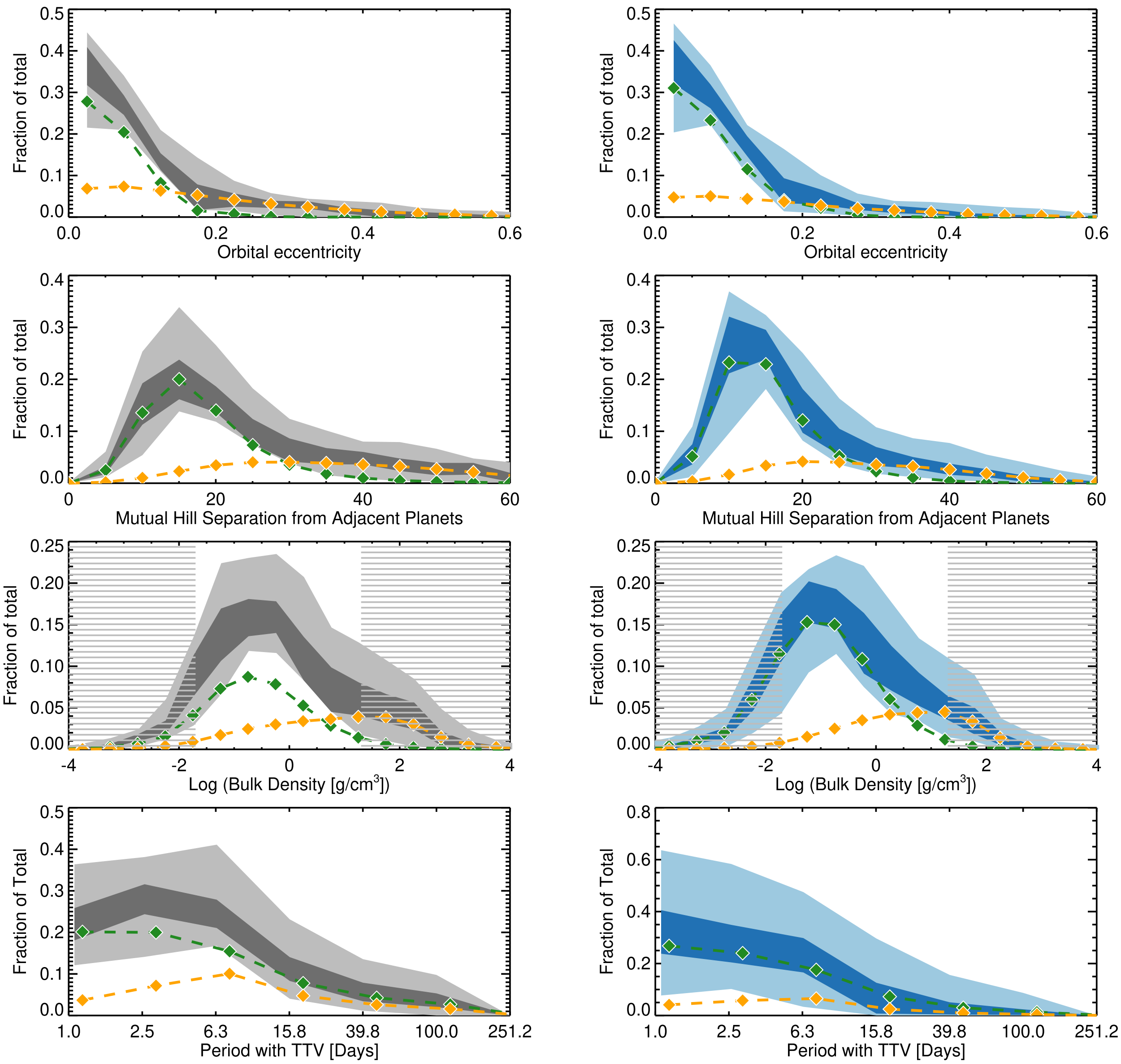

Figure 7. Resulting posterior distributions predicted for the *Kepler* mission at left (gray) and the *TESS* mission at right. In order from top to bottom: orbital eccentricity of detected planets, mutual Hill spacing from neighboring planets, predicted density from Hill spacing per Dawson et al. (2016), and periods of planets showing TTVs.

definition of "compact multiple" in Muirhead et al. (2015) is two or more planets interior to a 10 day orbit. Practically speaking, if planets are spaced equally in log semimajor axis, on average 5 $M_{\oplus}$, and dynamically stable, this corresponds to systems with seven or more planets interior to 200 days. This value is safely within the posterior distribution of number of planets per star N_1 found by Ballard & Johnson (2016): 40% of the distribution lies at seven planets per star or greater. Second, Muirhead et al. (2015) employed inverse detection efficiency machinery and compared the number of stars hosting two or more planets to the number hosting no planets. In comparison, in Ballard & Johnson (2016), we ignored entirely systems hosting no transiting planets. We employed forward modeling to compare models to a different observable altogether: the shape of the distribution in the number of transiting planets per star. We invert the posterior in f to $f_{\star}$ as follows.

For each 10^4 planetary systems we generate from the posterior on f (described in Section 2.2), we solve empirically for the fraction of stars $f_{\star}$ in Population 1. We make the assumption that every M dwarf in the sample hosts a planetary system of some kind, whether in Population 1 or 2, so that the fractions sum to 1. This assumption brings consistency between the mean number of planets per star of 2.0–2.5 determined by Morton & Swift (2014) and Dressing & Charbonneau (2015) and our planetary mixture model in which some stars host five planets and others host one, as we described in Ballard & Johnson (2016). We record this fraction $f_{\star}$ at each step of the MCMC chain. The lower panel of Figure 10 shows the resulting distribution in $f_{\star}$, as compared to results from Muirhead et al. (2015). While compact multiples make up 45% $\pm$ 10% of the transiting systems found by *Kepler*, they are only 15% $\pm$ 5% of all planetary systems orbiting early-M dwarfs. This is consistent with the 15.9% $\pm$ 1.5% found by Muirhead et al. (2015) for early-M dwarfs.

We compare in Figure 10 the resulting distributions in $f_{\star}$ between the *Kepler* and *TESS* missions. The selection bias that favored the detection of compact multiples from the *Kepler* mission is still greater for NASA's *TESS* mission. In the top

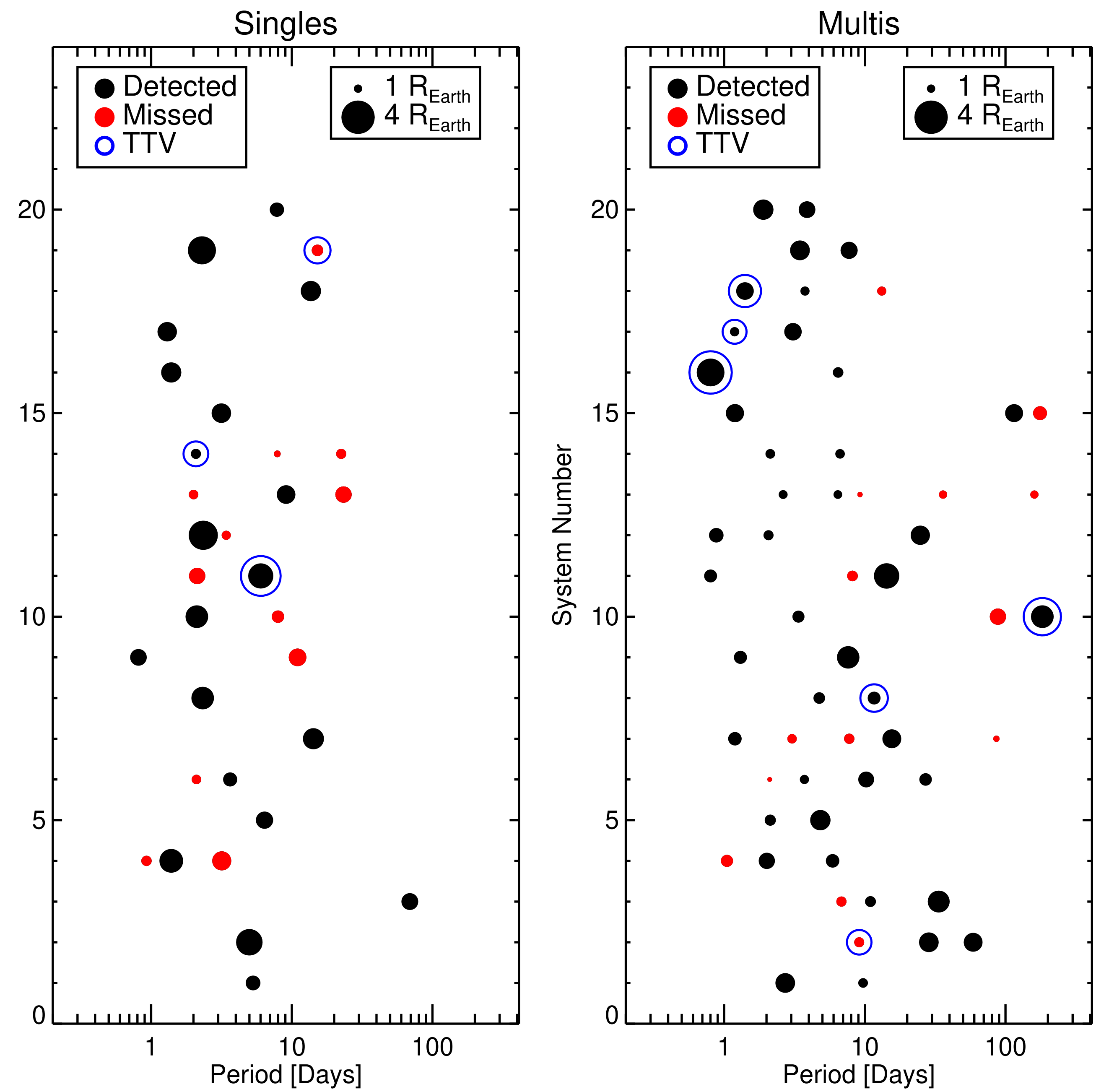

Figure 8. Left panel: representative sample of M-dwarf planetary systems in which *TESS* detected a single transiting planet. We depict only the transiting planets orbiting each star. Black indicates TESS-detected planets, while red indicates planets that were missed. Planet radii are shown by the relative sizes of the circles, while planets exhibiting TTVs are ringed in blue. Left panel: simple sample of systems in which *TESS* detected two or more transiting planets.

panel of Figure 10, we show the fraction of compact multis within the sample of planet hosts for both *Kepler* and *TESS*. Now the fraction f is 68% $\pm$ 12%, showing that the steep period completeness for *TESS* will likely result in 5$\times$ the rate of compact multiples among *TESS* hosts than the underlying rate in nature.

3.5. Implications for Ensemble Eccentricity

Orbital eccentricity in M-dwarf planetary systems has complicated implications for habitability. For the smallest stars, even a modest eccentricity can induce a sterilizing "runaway greenhouse" effect (Barnes et al. 2013). On the other hand, modest eccentricity may be sufficient to induce plate tectonics in the absence of radiogenic heating (Jackson et al. 2008). The eccentricity of a planet also shapes how we interpret its atmospheric signature (for a detailed summary, see Shields et al. 2016).

TESS's strong selection bias for shorter periods favors the discovery of compact and generally dynamically cooler systems, which we quantify in the previous section. This is particularly true for the multiple-planet systems uncovered by TESS, whose membership is almost certainly in this population. Figure 11 summarizes this result, showing the cumulative eccentricity distributions for both the single and multiple transiting systems. A comparison between the *TESS* and *Kepler* distributions shows the predicted lower eccentricity for *TESS* planetary systems on average. This effect is strongest for the multitransit systems from *TESS*, for which 80% of planets have

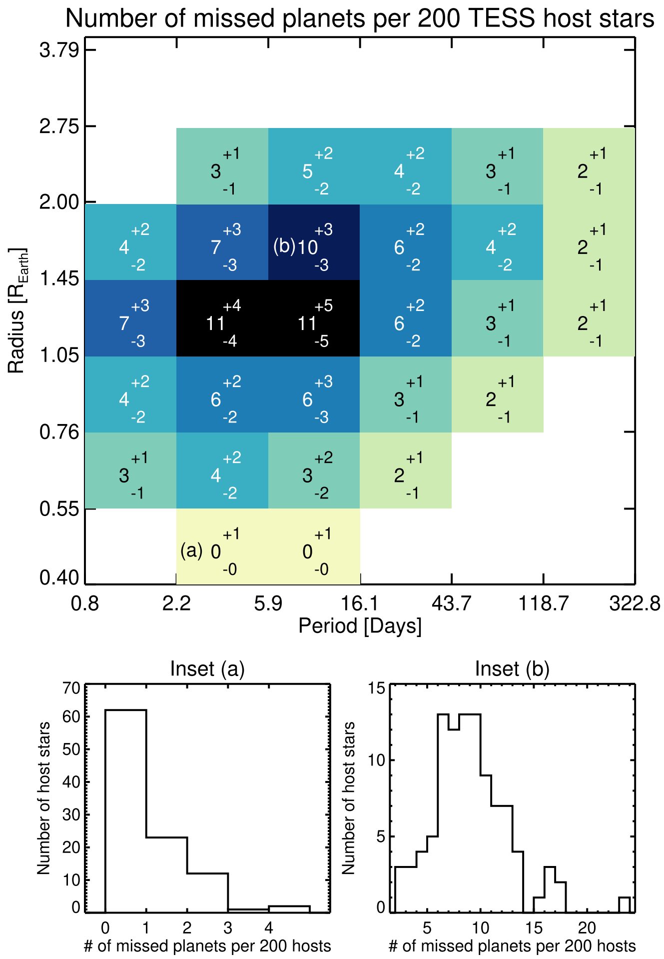

Figure 9. Top panel: for every 200 *TESS* host stars, the number of transiting planets below *TESS*'s detection threshold as a function of planetary radius and period. Bottom panels: Poisson distributions in number of missed planets per 200 host stars for two example bins, indicted by (a) and (b) in the top panel.

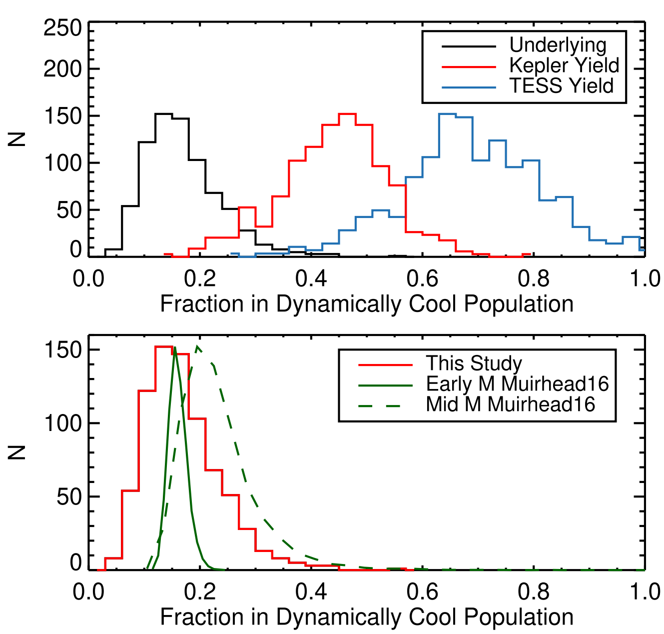

Figure 10. Top panel: fraction of "compact multiple"-type planetary systems in the underlying population, in the *Kepler* yield of detected planetary systems, and in the predicted TESS yield of detected planetary systems. Bottom panel: comparison between the underlying fraction of "compact multiple"-type planetary systems inferred from this work and from Muirhead et al. (2015).

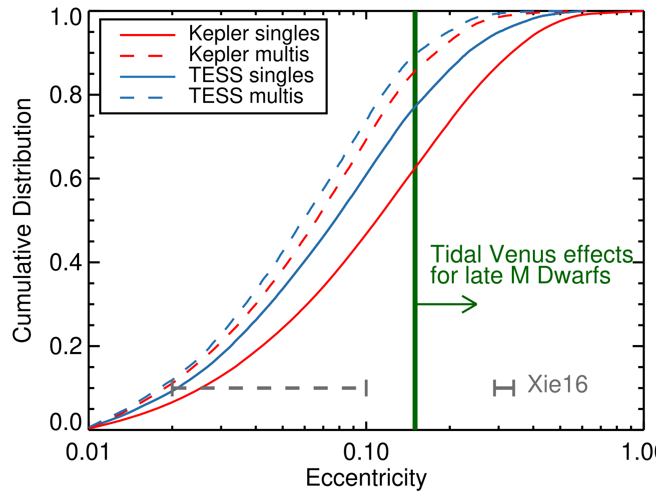

Figure 11. Predicted cumulative eccentricity distribution for both *TESS* (blue) and *Kepler* (red) missions, where planets in a system with a single detected planet (solid line) are shown separately from planets in systems with multiple detected planets (dashed line). We have overplotted in gray the empirical eccentricities measured for *Kepler*'s singles (dashed) and multis (solids) from Xie et al. (2016) for comparison.

orbital eccentricities less than 0.1. We overplot the empirical result of Xie et al. (2016) for the *Kepler* singles and multiples, measured from photometry. The eccentricities inferred for *Kepler* singles from this study are lower than the average measurement from Xie et al. (2016). However, we consider here the subset of M dwarfs rather than the full *Kepler* sample examined by Xie et al. (2016).

For the sake of comparison, we overplot an eccentricity associated with runaway tidal heating on late-M dwarfs from Barnes et al. (2013). There exists a range of cutoff eccentricities for this effect, depending upon bulk planet composition, atmospheric composition, and assumptions about exactly how the dynamical heating occurs. For this reason, the cutoff shown here is illustrative rather than definitive. We have depicted the cutoff eccentricity of 0.15 for the sake of comparison with the cumulative eccentricity distributions. For higher orbital eccentricities, planets 1 $M_\oplus$ and larger in the habitable zone of 0.25 $M_\odot$ stars are predicted to experience a runaway Venus effect (Barnes et al. 2013). We note that *TESS* planets are safer from this effect, on average, with the planets in multiplanet systems safest (with only 10% possessing orbital eccentricities greater than 0.15).

3.6. *TTVs*

While *TESS* itself may only rarely have the observational baseline to observe TTVs, we can predict their frequency among *TESS*-detected planets. Employing the empirical TTV likelihood as a function of the number of transiting planets from Xie et al. (2014), we predict the TTV likelihood among the *TESS* transiting planets. Figure 12 shows a comparison of the TTV fraction for both missions. In the *Kepler* sample, the overall rate of 5% reflects the mixture of planetary systems to which compact multis contribute only half. We show the TTV occurrence fraction from both populations in green (dynamically cool) and orange (dynamically hot), where the height of the histogram reflects the contribution of that population to the total number of planets. The *TESS* completeness, in contrast, heavily favors the types of compact multiples that exhibit TTVs. For *TESS*, these types of planetary systems will

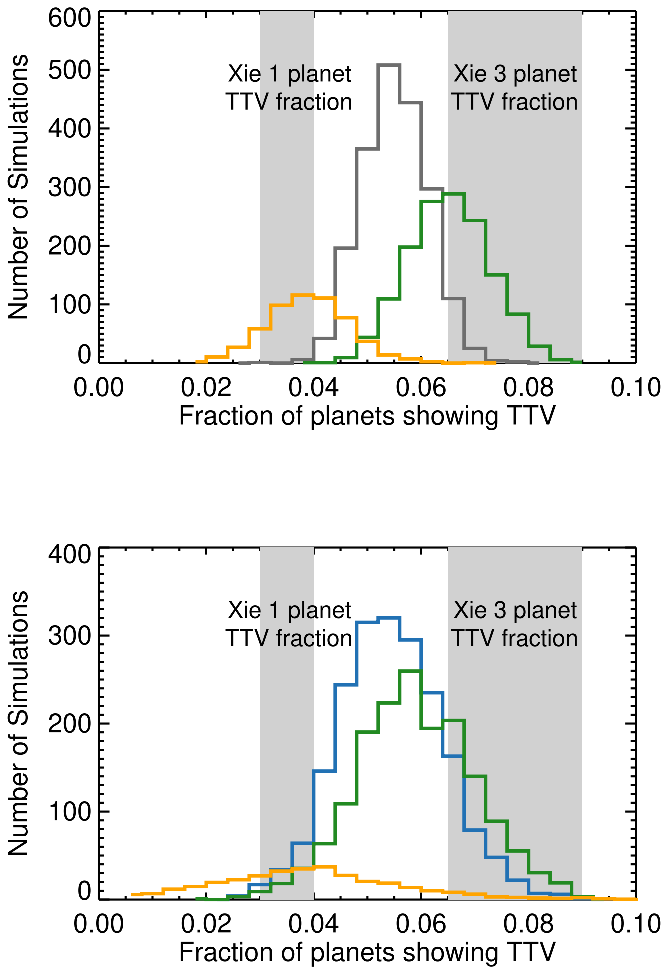

Figure 12. Top panel: posterior distribution for the fraction of *Kepler* planets (black) exhibiting TTVs, as defined by "Case 3" in Xie et al. (2014). The separate distributions for the dynamically cool (green) and dynamically hot (orange) populations have been scaled to reflect their relative contributions to the number of planets. Bottom panel: same distributions predicted for the *TESS* sample.

comprise a likely 70% of the yield, as we describe in the previous section. The fact that the final TTV rate is similar to *Kepler's* is due to a subtlety. Though compact multis are favored for detection by *TESS*, only one or two planets are typically detected in these systems, even if three or four transit. In comparison, consider the three and four transiting planet systems detected by *Kepler*. With the higher TTV probability per planet, the fact that there are three or four planets each with this higher probability (as opposed to one or two) skews the overall TTV likelihood higher. The trade-off between these two phenomena results in a TTV fraction similar to *Kepler*'s, despite *TESS*'s strong preference for compact multiples in which TTVs are more common.

3.7. Planet Bulk Density

The third panel of Figure 7 shows the posterior distribution in theoretical density assigned from mutual Hill spacing per Dawson et al. (2016). Only planets in systems for which Hill spacing is applicable (those with two or more planets) contribute to this distribution. We have indicated with cross-hatching the densities that are too high or low to be included in the Dawson et al. (2016) metric. The higher fraction of compact multiples within *TESS* and their accompanying close orbital spacing map to a predicted lower density, on average. Drawing from the entire predicted *TESS* yield for M-dwarf systems with two or more planets, we find $\bar{\rho} = 0.3^{+0.3}_{-0.1}$, which is likely 70% of the *TESS* planetary systems. The corresponding mean density for *Kepler* systems with two or more planets is $\bar{\rho} = 0.9^{+0.6}_{-0.4}$. This prediction for the average fluffiness of *TESS* planets will ultimately be tested with radial velocity follow-up and transmission spectroscopy; we leave the specific implications for those follow-up efforts for future work.

4. Summary and Conclusions

Using the injected and detected samples published by Sullivan et al. (2015), we have extracted a completeness function with planet radius and orbital period for *TESS* M dwarfs. We first demonstrate that the application of this completeness function to the Sullivan et al. (2015) injected planet sample correctly recovers the planet detections from that work. We then reapply the completeness function, assuming a different planet occurrence rate. Rather than assuming two to three planets per star, we assume a mixture model with two types of planetary systems. One type contains more than five closely aligned planets (around 20% of stars, per Section 3.4), and one contains one planet or two planets with high mutual inclination respective to one another. We return to our enumerated list of goals from Section 1 to summarize our findings on each.

1. We predict that *TESS* will uncover 1274 ± 241 planets orbiting 1026 ± 182 stars between 3200 and 4000 K, a factor of 1.2 more than predicted in Sullivan et al. (2015; Section 3.1). The error budget on the number of detections is dominated by uncertainty on the underlying fraction of compact multiples in nature.
2. Even given the typical duration of 27 days per star, we predict that *TESS* will detect two or more planets around 189 ± 66 stars among the hosts above. The approximately 20% contribution of multis to the total host star budget is similar to *Kepler* M dwarfs. The high rate of compact multiples indicates that *TESS* will even detect three or more planets around 45 ± 22 stars (Section 3.2).
3. Among 200 typical *TESS* M-dwarf host stars, an average of 250 planets will be detectable in the mission data themselves. We predict that half that number lurk below the mission sensitivity: 93 ± 17 planets per 200 host stars. Many of these planets will be readily detectable from ground-based surveys and space-based campaigns (Section 3.3)
4. We confirm the compact multiple rate (defined as two or more planets with orbital periods <10 days) among M dwarfs measured previously in the literature. We find this rate to be 15% ± 5% among early-M dwarfs, as compared to 15.9% ± 1.5% (Muirhead et al. 2015) using a different technique. While compact multiple hosts are not the majority in nature, the relative ease of their detection makes them overrepresented in transit surveys: they are 45% ± 10% of *Kepler*-detected planet hosts, and we predict that they will be 68% ± 12% of *TESS*-detected planet hosts.
5. By virtue of the lower average eccentricities of planets in multiple-planet systems, we predict that the average orbital eccentricity of planets detected by *TESS* will be

correspondingly lower than the average for *Kepler*. For systems in which *TESS* detects two or more transiting planets, 80% of planets will have orbital eccentricities less than 0.1.

6. Despite the higher fraction of compact multiples in the *TESS* yield, the number of planets detected by *TESS* that exhibit TTVs (as defined by Xie et al. 2014) will be similar to the overall 5% observed for *Kepler*. These TTVs will not be detectable by *TESS* itself as for *Kepler*, but we predict that the underlying rate among detected planets will be similar.
7. Employing the planet formation theory of Dawson et al. (2016) linking adjacent planet spacing to planet bulk density, we predict that *TESS* planets will be fluffier, on average. We apply this metric to systems with at least two planets to find $\bar{\rho} = 0.3^{+0.3}_{-0.1}$ among *TESS* planets, as compared to $\bar{\rho} = 0.9^{+0.6}_{-0.4}$ for *Kepler* planets (Section 3.7.)

We conclude by reemphasizing the ground- and space-based opportunity for photometric follow-up specific to planet discovery. Around stars for which *TESS* detects one or more planets, we predict a wealth of additional transiting planets present but undetectable in the *TESS* light curves (Section 3.3). We take as an example a hypothetical survey of 200 *TESS* host stars sensitive to 1 $R_\oplus$ planets and with 100% completeness out to only 2.2 days. Such a study will detect 11 $\pm$ 5 additional planets. The odds improve yet more if *TESS* has detected two or more planets around the star or if one of the planets exhibits TTVs. An extended *Spitzer* mission (as detailed by Yee et al. 2017) would have the photometric sensitivity time baseline to be sensitive to rocky planets, even in the habitable zone of *TESS* hosts. While we predict that *TESS* itself will detect 4^{+3}_{-2} planets $<1.25\,R_\oplus$ with orbital periods 20 days $< P <$ 40 days, an additional 21 $\pm$ 7 such planets will orbit known *TESS* hosts to another transiting planet but elude detection by *TESS* proper. An extended *Spitzer* mission may be singularly suited for their discovery.

The soon-to-be-launched *CHaracterising ExOPlanet Satellite* (*CHEOPS*; Fortier et al. 2014) will gather high-precision transit observations to constrain (among many objectives) planetary atmospheres and formation. The telescope, in a geocentric orbit, will continuously point at a single target for typically 6–12 hr; however, it can achieve stares of a few weeks' duration (Broeg et al. 2013) and, in principle, could also readily detect additional planets. Additionally, ground-based photometric surveys such as MEarth (Nutzman & Charbonneau 2008) and TRAPPIST (Gillon et al. 2011) have already demonstrated the ability to detect planets $<2\,R_\oplus$ orbiting M dwarfs (Charbonneau et al. 2009; Berta-Thompson et al. 2015; Dittmann et al. 2017; Gillon et al. 2017). The forthcoming wealth of *TESS* planets portends a strong synergy with follow-up efforts.

We thank Philip Muirhead, Joshua Winn, and particularly John Johnson for discussions that immeasurably improved this manuscript. S.B. is funded by the MIT Torres Fellowship for Exoplanet Science.

References

Ballard, S., & Johnson, J. A. 2016, ApJ, 816, 66
Barnes, R., Mullins, K., Goldblatt, C., et al. 2013, AsBio, 13, 225
Berta, Z. K., Irwin, J., & Charbonneau, D. 2013, ApJ, 775, 91
Berta-Thompson, Z. K., Irwin, J., Charbonneau, D., et al. 2015, Natur, 527, 204
Bonfils, X., Delfosse, X., Udry, S., et al. 2013, A&A, 549, A109
Bovaird, T., & Lineweaver, C. H. 2017, MNRAS, 468, 1493
Bowler, B. P., Liu, M. C., Shkolnik, E. L., & Tamura, M. 2015, ApJS, 216, 7
Boyajian, T. S., von Braun, K., van Belle, G., et al. 2012, ApJ, 757, 112
Broeg, C., Fortier, A., Ehrenreich, D., et al. 2013, EPJWC, 47, 03005
Buchner, J., Georgakakis, A., Nandra, K., et al. 2014, A&A, 564, A125
Charbonneau, D., Berta, Z. K., Irwin, J., et al. 2009, Natur, 462, 891
Christiansen, J. L., Clarke, B. D., Burke, C. J., et al. 2016, ApJ, 828, 99
Clanton, C., & Gaudi, B. S. 2016, ApJ, 819, 125
Dawson, R. I., Lee, E. J., & Chiang, E. 2016, ApJ, 822, 54
Dittmann, J. A., Irwin, J. M., Charbonneau, D., et al. 2017, Natur, 544, 333
Dressing, C. D., & Charbonneau, D. 2013, ApJ, 767, 95
Dressing, C. D., & Charbonneau, D. 2015, ApJ, 807, 45
Fabrycky, D. C., Ford, E. B., Steffen, J. H., et al. 2012a, ApJ, 750, 114
Fabrycky, D. C., Lissauer, J. J., Ragozzine, D., et al. 2012b, ApJ, 790, 146
Feroz, F., & Hobson, M. P. 2008, MNRAS, 384, 449
Feroz, F., Hobson, M. P., & Bridges, M. 2009, MNRAS, 398, 1601
Feroz, F., Hobson, M. P., Cameron, E., & Pettitt, A. N. 2013, arXiv:1306.2144
Foreman-Mackey, D., Hogg, D. W., & Morton, T. D. 2014, ApJ, 795, 64
Fortier, A., Beck, T., Benz, W., et al. 2014, Proc. SPIE, 9143, 91432J
Gaidos, E., Mann, A. W., Kraus, A. L., & Ireland, M. 2016, MNRAS, 457, 2877
Gardner, J. P., Mather, J. C., Clampin, M., et al. 2006, SSRv, 123, 485
Gillon, M., Jehin, E., Magain, P., et al. 2011, EPJWC, 11, 06002
Gillon, M., Triaud, A. H. M. J., Demory, B.-O., et al. 2017, Natur, 542, 456
Hawkins, D. M. 1994, Computational Statistics, Vol. 9 (Amsterdam: Elsevier)
Howard, A. W., Marcy, G. W., Bryson, S. T., et al. 2012, ApJS, 201, 15
Hsu, D. C., Ford, E. B., Ragozzine, D., & Morehead, R. C. 2018, AJ, 155, 205
Jackson, B., Greenberg, R., & Barnes, R. 2008, ApJ, 678, 1396
Johnson, J. A., Aller, K. M., Howard, A. W., & Crepp, J. R. 2010, PASP, 122, 905
Limbach, M. A., & Turner, E. L. 2015, PNAS, 112, 20
Lissauer, J. J., Ragozzine, D., Fabrycky, D. C., et al. 2011, ApJS, 197, 8
Mills, S. M., & Mazeh, T. 2017, ApJL, 839, L8
Montet, B. T., Crepp, J. R., Johnson, J. A., Howard, A. W., & Marcy, G. W. 2014, ApJ, 781, 28
Moriarty, J., & Ballard, S. 2016, ApJ, 832, 34
Morton, T. D., & Swift, J. 2014, ApJ, 791, 10
Morton, T. D., & Winn, J. N. 2014, ApJ, 796, 47
Muirhead, P. S., Mann, A. W., Vanderburg, A., et al. 2015, ApJ, 801, 18
Mulders, G. D., Pascucci, I., & Apai, D. 2015, ApJ, 814, 130
Murray, K., Müller, S., & Turlach, B. A. 2013, Computational Statistics, 28, 1989
Nutzman, P., & Charbonneau, D. 2008, PASP, 120, 317
Petigura, E. A., Howard, A. W., & Marcy, G. W. 2013a, PNAS, 110, 19273
Petigura, E. A., Marcy, G. W., & Howard, A. W. 2013b, ApJ, 770, 69
Ricker, G. R., Winn, J. N., Vanderspek, R., et al. 2014, Proc. SPIE, 9143, 914320
Rogers, L. A. 2015, ApJ, 801, 41
Shields, A. L., Ballard, S., & Johnson, J. A. 2016, PhR, 663, 1
Sullivan, P. W., Winn, J. N., Berta-Thompson, Z. K., et al. 2015, ApJ, 809, 77
Tarter, J. C., Backus, P. R., Mancinelli, R. L., et al. 2007, AsBio, 7, 30
Turlach, B. A., & Murray, K. 2016, MonoPoly: Functions to Fit Monotone Polynomials, r Package Version 0.3-8
Vanderspek, R., Huang, C. X., Vanderburg, A., et al. 2018, arXiv:1809.07242
Wolfgang, A., Rogers, L. A., & Ford, E. B. 2016, ApJ, 825, 19
Xie, J.-W., Dong, S., Zhu, Z., et al. 2016, PNAS, 113, 11431
Xie, J.-W., Wu, Y., & Lithwick, Y. 2014, ApJ, 789, 165
Yee, J. C., Fazio, G. G., Benjamin, R., et al. 2017, arXiv:1710.04194
Youdin, A. N. 2011, ApJ, 742, 38
Zeng, L., & Jacobsen, S. B. 2017, ApJ, 837, 164